Desalination and Water Treatment
www.deswater.com
doi: 10.5004/dwt.2020.25447

185 (2020) 111–123
May

Study on horizontal jets with buoyancy in shallow waters

Jie Song[a,b,c], Mingtao Jiang[d], Myung Eun Lee[e], Adrian Wing-Keung Law[d,f,*]

[a]*Shanghai Environmental Protection Key Laboratory on Environmental Standard and Risk Management of Chemical Pollutants, East China University of Science & Technology, Shanghai 200237, China,*
[b]*NTU-Hyundai Urban System Centre, Hyundai Engineering and Construction Co. Ltd., 1 CleanTech Loop, Singapore 637141*
[c]*Shanghai Institute of Pollution Control and Ecological Security, Shanghai 200092, China*
[d]*Environmental Process Modelling Centre, Nanyang Environment and Water Research Institute (NEWRI), Nanyang Technological University, 1 CleanTech Loop, Singapore 637141, emails: cwklaw@ntu.edu.sg (A. Wing-Keung Law), mtjiang@ntu.edu.sg (M. Jiang)*
[e]*Hyundai Engineering and Construction Co. Ltd., R&D Division, Jongno-Gu, Republic of Korea, email: melee@hdec.co.kr (M. Eun Lee)*
[f]*School of Civil and Environmental Engineering, Nanyang Technological University, 50 Nanyang Avenue, Singapore 639798*

Received 6 August 2019; Accepted 1 January 2020

ABSTRACT

Submerged outfalls are widely used by coastal industrial facilities for effluent discharges. To minimize the construction cost, the outfall may be situated in relatively shallow waters, whereby the dilution is influenced by the bounded water surface and seabed together. In this case study, the mixing characteristics of horizontal jets with either positive or negative buoyancy were investigated in shallow coastal waters. The arrangement mimicked the design configuration for a large coastal facility with co-located liquefied natural gas and power generation. Both numerical simulations and experiments were carried out to examine the jet characteristics. The large eddy simulation (LES) approach with the Smagorinsky sub-grid closure was adopted in the numerical simulations. Corresponding experimental measurements were performed using the planar laser induced fluorescence technique. The results showed that the potential core of the bounded jets with buoyancy was shortened with this configuration compared to the unbounded free jets. The LES simulations were able to reproduce the geometric characteristics of the buoyant jet under the confinement of the water surface and seabed in a satisfactory manner. However, the predictions on the jet spread were relatively conservative and the minimum dilution was underestimated by about 20%–30% on average, which can be taken into account by the design calculations.

Keywords: Buoyant jets; Shallow waters; LES; PLIF

1. Introduction

Submerged outfalls are widely used in coastal industrial facilities due to their superior dilution performance compared to surface outfalls [1–3]. For dense effluents having a heavier density than the ambient environment [e.g., brine with higher salinity from desalination plants and de-cooling water with lower temperature from liquefied natural gas (LNG) plants], an inclined submerged outfall is normally applied. On the other hand, for effluents with a lighter density, that is, cooling water from power plants, a horizontal submerged outfall is adopted with the jets rising upward to the water surface due to buoyancy [4]. Many studies have now been conducted to investigate the performance of submerged outfalls through both analytical and experimental means. For example, integral models have been developed and widely used, for example, Cormix, Visjet, and Visual Plumes [5–8]. Laboratory experiments have been conducted by using different techniques to measure the characteristics and dilution behaviors as well [9–12].

* Corresponding author.

Most of the previous studies focused on examining the jet characteristics and dilution performance in unbounded conditions. In reality, the submerged outfall may need to be built in a coastal area with a shallow water depth due to flat topography and economical reasons [13]. In such cases, the jet development would be affected by the presence of the water surface and seabed. In earlier years, experimental studies had been conducted to investigate the behavior of non-buoyant jets in shallow waters. Chen and Jirka [14] applied the technique of laser induced fluorescence to examine the mixing performance of a plane non-buoyant jet in shallow waters. The concentration properties of the jet were found to be related to the water depth. Raiford and Khan [15] measured the velocity field of a non-buoyant circular jet in shallow waters using a Prandtl tube. They found that the velocity profiles in the horizontal plane were similar in general, while that in the vertical plane were similar only in the area close to the nozzle. Shinneeb et al. [16] examined the velocity and turbulence characteristics of non-buoyant circular jets in shallow waters using the technique of particle image velocimetry. The entrainment in the vertical direction was found to be suppressed by the presence of the water surface.

Compared to non-buoyant jets, situations of jets with buoyancy are more complicated. The definition of shallow waters differs between positively and negatively buoyant effluents. With positive buoyancy, the constraints by the water surface can induce instability in the flow pattern. Johnston and Volker [17] and Sobey et al. [18] studied horizontal round buoyant jets in shallow waters through experimental approaches. Their results were found to differ from the predictions by integral models for an unbounded environment. Jiang et al. [19] conducted experiments to study inclined dense jets with the inclination angles of 30° and 45° in shallow waters. They found that the surface constraint lengthens the jet-spreading distance, but the return point dilution is roughly the same as in deeper water. Shao and Law [20,21] examined the turbulent mass transport and boundary interactions of horizontal offset dense jets experimentally, respectively. In addition, some studies on the initial dilution of thermal effluent discharges with different water depths and outfall configurations had been reported in the literature. The impingement point distances under various conditions were examined experimentally [22–24].

In recent years, due to the fast development of computational techniques, numerical simulations have now been widely used to provide predictions in many engineering applications. For the discharge of effluents, there have been some studies reported on submerged jets in unbounded conditions through computational fluid dynamic (CFD) simulations [25–27]. However, numerical simulations on the characteristics and dilution behavior of submerged horizontal jets in shallow waters are relatively rare. Recently, Chowdhury et al. [28] studied non-buoyant circular jets in shallow waters using the software Fluent. It was found that the jet trajectory tends to shift toward the closest confining surface.

In this study, horizontal offset jets with a three-port configuration in shallow waters with both positive and negative buoyancy were studied through numerical approaches. Laboratory experiments using planar laser induced fluorescence (PLIF) were also conducted to evaluate the numerical predictions. In the discharged configuration, the port height (i.e., distance between the port center and bed) was ~3 and 6 D, the water depth above the port (i.e., distance between the port center and free surface) ranged from 3 to 9 D, and the spacing between each port was 15 D, where D is the port diameter. This configuration mimicked the effluent discharge through a prototype co-located power and LNG plant. In the experiments, the jet spread began to impinge the confined boundaries after a distance of ~20–30 D. It should be noted that the port spacing was relatively large while the impinging distance was relatively short in this case, hence the merging effect of the three jets was not addressed in the present study. We note that in real engineering applications, it is common that the submerged outfalls have to be built in shallow water areas due to land and economical constraints. In such conditions, integral models (e.g., Visjet) which are developed for an unbounded environment might not be able to provide satisfactory predictions to the engineering calculations and design. Hence, this study is performed to explore the feasibility of applying CFD simulations to tackle outfall designs in shallow waters which are difficult to be handled by conventional integral models. As far as we are aware, it is the first time that the large eddy simulation (LES) approach was adopted to investigate horizontal jets with buoyancy in shallow waters for real engineering design. The experimental and numerical setup are first described in the following. Subsequently, the results are summarized and discussed.

2. Experimental study

Experiments were conducted in a water flume with 6.4 m length, 1.0 m width, and 0.7 m height, located at the environmental process modeling center lab, Nanyang Technological University, Singapore. Fig. 1 shows the schematic diagram of the experimental setup. During the experiments, the flume was partially filled with tap water at room temperature (i.e., around 25°C, $\rho \approx 997$ kg/m^3), which acted as the static ambient. A model was fabricated to discharge the effluents, which mimicked the configuration of a real submerged outfall system constructed by Hyundai Engineering and Construction (Bldg., 75, Yulgok-ro, Jongro-gu, Seoul 03058). The port inner diameter was 8 mm and the spacing between each port was 120 mm; hence, the merging effect was not obvious in the near field area due to the relatively large spacing distance. The flowrate of each port could be adjusted independently through internal valves. Before the test, the flowrate of each port was measured independently to ensure consistency.

The varying density of the effluent was achieved by changing the temperature of the discharged water. The heated/cooled water was supplied by a water circulating container (model: PolyScience, AD28R-30-A12E, 6600 W. Touhy Avenue, Niles, Illinois 60714-4516 USA), in which the water can be heated/cooled to the desired temperature and maintained during the experiments. The density differences between the ambient water and effluent ranged from –0.34% to 0.43%. A dual-head peristaltic pump (model: MasterFlex, 77200-62, Willy-Brandt-Allee 300, 45891 Gelsenkirchen, Germany) with an adjustable flowrate was used to transport the water from the container to the model, and subsequently discharged into the water flume. Before each test, the temperature and density of the water in both the container and water flume were carefully measured by a thermometer/

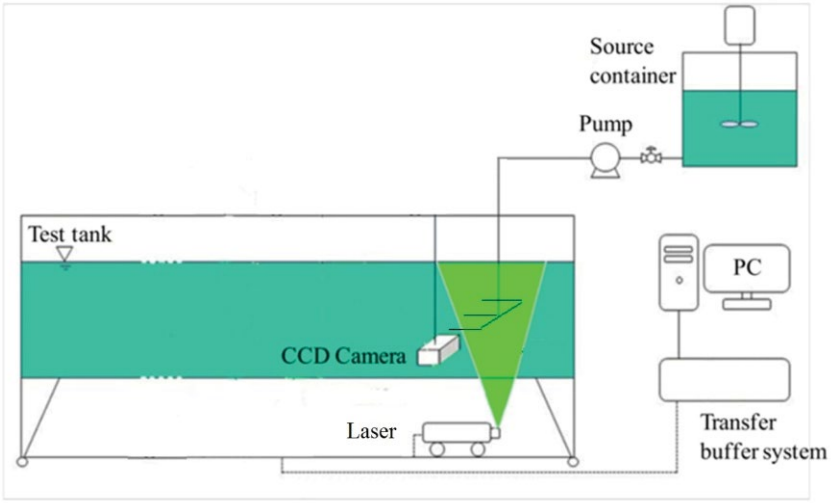

Fig. 1. Schematic diagram of experimental setup.

densimeter (model: Anton Paar, DMA 35N, Karntner Strasse 324 Graz, 8054 Austria). As the distance from the water container to the discharge point was <1 m and the water transport tubing was fully covered by thermal-insulating materials, the temperature of the discharged effluent can be considered to be the same as that in the water container.

PLIF was applied to quantitatively examine the jet characteristics and dilution behavior. It is a laser technique which can determine the instantaneous scalar distribution fields using fluorescent dye [29]. In the experiment, the laser used was a dual-cavity pulsed laser (model: Dantec Dynamics, DualPower 50–100 Laser, 16–18 Tonsbakken DK-2740 Skovlunde, Denmark). A high speed charge-coupled device digital camera (model: Dantec Dynamics, SpeedSense 1040) was employed to capture the images. Rhodamine 6G was used as the fluorescent dye as it is relatively stable under different temperatures [30]. Calibration was performed to obtain the relationship between the fluorescence light and dye concentration before each experiment.

To prepare for the experiments, a certain amount of dye was mixed with the water in the container to produce the source solution with a specific concentration. The laser light was then introduced from the bottom of the flume, which was adjusted to illuminate the center plane of the middle port. After the jet reached the steady state, the camera began to capture images in front of the flume. The image capture frequency was set to be 20 Hz and the duration lasted 30 s for each test (i.e., 600 pictures). The measured distance was about 250 mm. The captured images were later analyzed using the calibration curve by the software Dynamic Studio to obtain the concentration maps.

The test conditions were set by varying the effluent temperature, flowrate, and water depth as listed in Table 1, where the variables include u_0, T_e, h, and d. Here u_0 is the jet exit velocity, T_e and T_a are the effluent and ambient water temperature, respectively, h the distance between port center and bottom, and d the distance from port center to water surface. In the present study, the temperature difference (i.e., T_e–T_a) was set to be ±10°C, h ranged from 25 to 50 mm, and d from 25 to 75 mm. The densimetric Froude number and Reynolds number are calculated by:

$$\mathrm{Fr} = \frac{u_0}{\sqrt{\left|\frac{\Delta\rho}{\rho_a}\right| gD}} \tag{1}$$

Table 1
Experimental conditions

Case	u_0 (m/s)	T_e (°C)	h (m)	d (m)	Δρ (kg/m³)	Fr	Re	L_M (m)	Bed proximity h/L_M
1	0.498	T_a+10°C	0.025	0.075	–3.4	30.7	4,945	0.231	0.108
2	0.498	T_a+10°C	0.025	0.025	–3.4	30.7	4,945	0.231	0.108
3	0.498	T_a+10°C	0.050	0.050	–3.4	30.7	4,945	0.231	0.216
4	0.398	T_a+10°C	0.025	0.075	–3.4	24.6	3,956	0.185	0.135
5	0.398	T_a+10°C	0.025	0.025	–3.4	24.6	3,956	0.185	0.135
6	0.498	T_a–10°C	0.025	0.075	4.3	27.2	3,048	0.205	0.122
7	0.498	T_a–10°C	0.025	0.025	4.3	27.2	3,048	0.205	0.122
8	0.498	T_a–10°C	0.050	0.050	4.3	27.2	3,048	0.205	0.244

$$\mathrm{Re} = \frac{u_0 D}{\nu} \tag{2}$$

where ν is the kinematic viscosity, $\Delta\rho$ the density difference between the effluent and ambient water, g the gravitational acceleration, and ρ_a the ambient density. The experimental conditions were chosen such that (1) the dimensions were scaled down according to that of the real project configuration, (2) Re was larger than 3,000 to ensure fully turbulent flows, and (3) Fr was comparable to that of the jet characteristics in the prototype.

3. Computational methodology

A CFD study was performed to simulate submerged horizontal jets with positive/negative buoyancy in shallow waters. In this study, the LES approach was adopted. By using LES, the large-scale eddies were computed by resolving the instantaneous Navier–Stokes equations directly, while the small-scale ones were modeled with a sub-grid model.

3.1. Governing equations

With the LES approach, the continuity, momentum, and transport equations of the large-scale eddies are as follows [31]:

$$\frac{\partial \rho}{\partial t} + \frac{\partial}{\partial x_j}\left(\rho \tilde{u}_j\right) = 0 \tag{3}$$

$$\frac{\partial}{\partial t}\left(\rho \tilde{u}_i\right) + \frac{\partial}{\partial x_j}\left(\rho \tilde{u}_i \tilde{u}_j\right) = -\frac{\partial p}{\partial x_i} + \frac{\partial}{\partial x_j}\left[\mu\left(\frac{\partial \tilde{u}_i}{\partial x_j}\right)\right] + \frac{\partial \tau_{ij}}{\partial x_j} \tag{4}$$

$$\frac{\partial}{\partial t}\left(\rho \tilde{\phi}\right) + \frac{\partial}{\partial x_j}\left(\rho \tilde{\phi} \tilde{u}_j\right) = \frac{\partial}{\partial x_j}\left[\Gamma\left(\frac{\partial \tilde{\phi}}{\partial x_j}\right)\right] + \frac{\partial Q_j}{\partial x_j} \tag{5}$$

where u_i, u_j are the velocity in i, j direction, respectively; p is the pressure, ρ is the fluid density, μ is the fluid viscosity, t is the time, Γ is the scalar diffusivity, and ϕ is the scalar concentration. The tilde indicates spatially filtered variables; $\tau_{ij} = -\rho\tilde{u}_i\tilde{u}_j - \rho\tilde{u}_i\tilde{u}_j$ and $Q_j = -\rho\tilde{\phi}\tilde{u}_j - \rho\tilde{\phi}\tilde{u}_j$ are sub-grid scale (SGS) stresses and SGS scalar flux, respectively.

For the small-scale eddies, the sub-grid turbulence closures are used, which is based on the Boussinesq hypothesis, and the sub-grid turbulent stresses are computed as:

$$\tau_{ij} - \frac{1}{3}\tau_{kk}\delta_{ij} = -2\mu_t \tilde{S}_{ij} \tag{6}$$

$$Q_j = \frac{\mu_t}{\mathrm{Sc}_t}\frac{\partial \tilde{\phi}}{\partial x_j} \tag{7}$$

where μ_t is the SGS viscosity, τ_{kk} the isotropic part of the SGS stresses, Sc_t the turbulent Schmidt number, which can be taken as 0.7 [32], δ_{ij} the kronecker delta, and $\tilde{S}_{ij}$ the strain rate tensor calculated by:

$$\tilde{S}_{ij} = \frac{1}{2}\left(\frac{\partial \tilde{u}_i}{\partial x_j} + \frac{\partial \tilde{u}_j}{\partial x_i}\right) \tag{8}$$

In the present study, the Smagorinsky SGS model was applied to solve for the SGS viscosity μ_t [31,33],

$$\mu_t = \rho L_S^2 \left|\tilde{S}\right| \tag{9}$$

where $\left|\tilde{S}\right| \equiv \sqrt{2\tilde{S}_{ij}\tilde{S}_{ij}}$ and L_S is the mixing length defined by:

$$L_S = \min\left(\kappa d_{\mathrm{wall}}, C_S \Delta\right) \tag{10}$$

where $\kappa = 0.4$ is the Von Karman constant, d_{wall} the distance to the wall, Δ the grid length, and C_S the Smagorinsky constant which was set to be 0.17 in this study [26].

3.2. Computational setup

To numerically solve the above equations, they were firstly discretized through the finite volume method and the open source software—OpenFOAM was applied to perform the simulations. The solver twoLiquidMixingFoam was adopted in this study, where two incompressible fluids with different densities were considered. The dimensions of the computational domain were 500 mm (L) × 640 mm (W) × 50/100 mm (H), where the boundaries in the longitudinal and lateral directions were sufficiently far away from the interested area.

The geometry of the discharge configuration in the numerical setup was set to be the same to the experiments. Three circular nozzles with diameter of 8 mm were embedded into the domain by using snappyHexMesh at different heights in accordance to the experimental conditions. The grid spacing increased from the nozzle center to the boundaries with stretch ratios ranged from 1.02 to1.05 in different directions. Furthermore, a double-refined mesh was performed close to the area of each nozzle outlet in order to cover the potential cores. The averaged grid size at the outlet was ~O(10^{-8}) m, and the number of grids on the outlet surface was about 200. The meshes of the computational domain as well as the nozzle outlet are shown in Fig. 2.

Open boundary condition (i.e., zero gradient) was used for the left, right, front, and back boundaries, and free surface for the top boundary. Wall function was applied to the bottom and circular boundaries of the nozzles. A uniform velocity inlet with a turbulence intensity of 10% was used for the discharge surface of the nozzles. The simulation conditions (i.e., density, exit velocity, etc.) were also set to be the same as the experimental conditions. An upwind scheme was applied to solve the divergence term, a linear scheme was used to compute the Laplacian term, and a second order implicit backward scheme was chosen for the temporal term. The time step interval was set to be auto-adjusted to ensure that the Courant number was not more than 1. The convergence criterion was 10^{-6} for the continuity, velocities, and scalar concentrations. To examine the grid convergence, simulation results under different grid size were analyzed and compared, and the conclusions of Zhang et al. [26] were

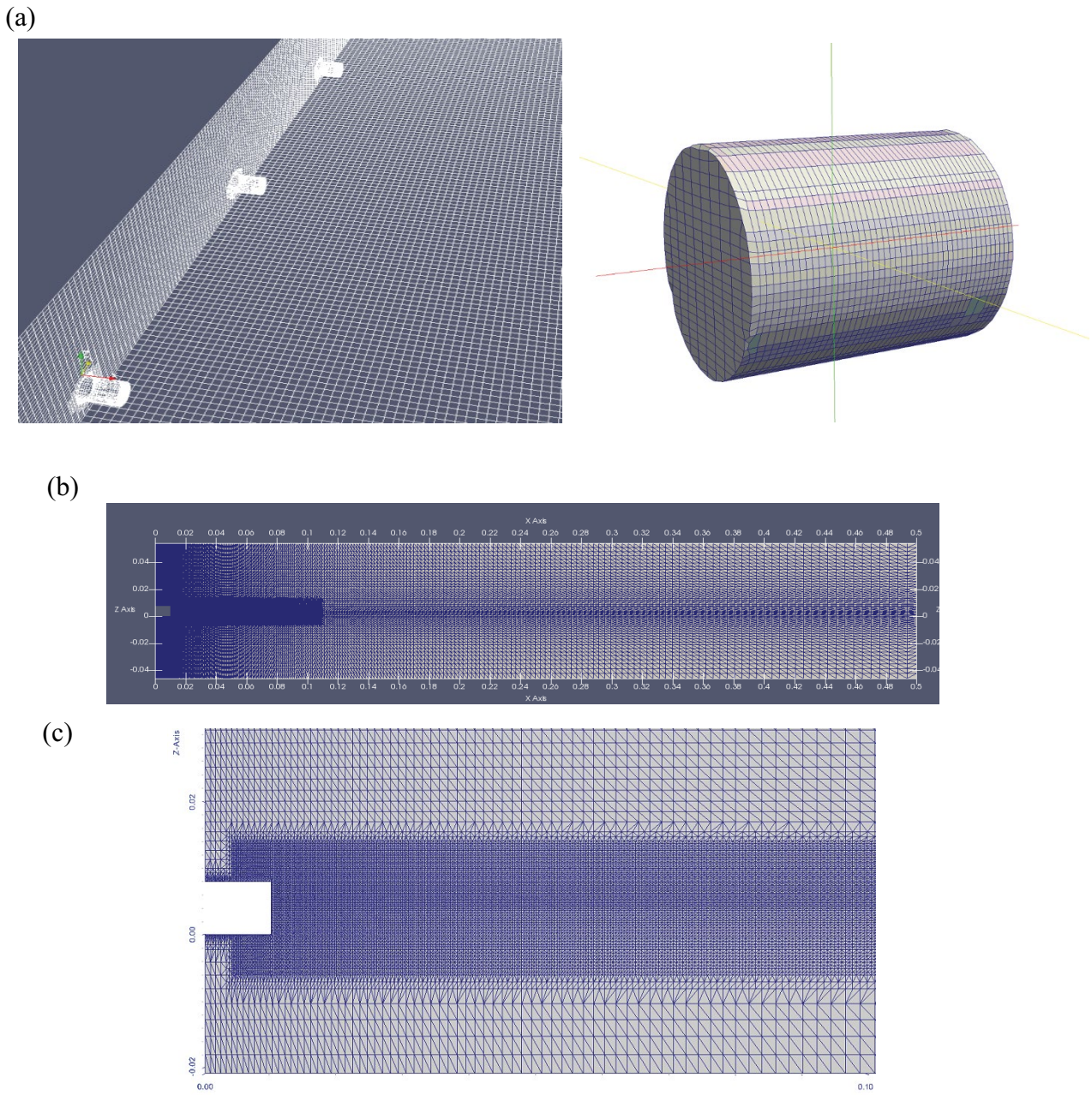

Fig. 2. Mesh of computational domain. (a) Mesh of nozzles, (b) mesh of domain, and (c) zoomed-in mesh of nozzle area.

taken into consideration. The total grid number was chosen to be 7–8 million for the cases of 100 mm height and 5–6 million for that with 50 mm height, respectively. The simulation time was set to be 30 s which is sufficient for the jet to reach steady state. The detailed numerical conditions are listed in Table 2.

4. Results and discussion

4.1. Flow characteristics

Firstly, the average jet characteristics were analyzed and compared qualitatively. Figs. 3 and 4 show the instantaneous and time-averaged concentration contour at the centerline plane of the middle jet of Case 1 (positively buoyant) and Case 7 (negatively buoyant) by experimental observation and CFD simulations, respectively, with the CFD prediction results obtained by averaging from 25 to 30 s, and the experimental results averaged over 600 images. It can be seen that the jet core was maintained steadily for a distance of $x/D \approx 3$ after the discharge. As the jet developed, the potential core diminished and finally disappeared due to the entrainment of the ambient water. Further downstream, the jet moved upward or downward depending on the buoyancy, and finally impingement occurred at the water surface or the bed which confined the expansion of the jet streamwise. By

Table 2
Numerical conditions

Case	u_0 (m/s)	h (m)	d (m)	Δρ (kg/m^3)	Number of computing CPU cores	Number of cells (million)	Run time for 30s (day)
1	0.498	0.025	0.075	–3.4	16	7.2	9
2	0.498	0.025	0.025	–3.4	16	5.6	7
3	0.498	0.050	0.050	–3.4	16	7.8	9
4	0.398	0.025	0.075	–3.4	16	7.2	9
5	0.398	0.025	0.025	–3.4	16	5.6	7
6	0.498	0.025	0.075	4.3	16	7.2	9
7	0.498	0.025	0.025	4.3	16	5.6	7
8	0.498	0.050	0.050	4.3	16	7.8	9

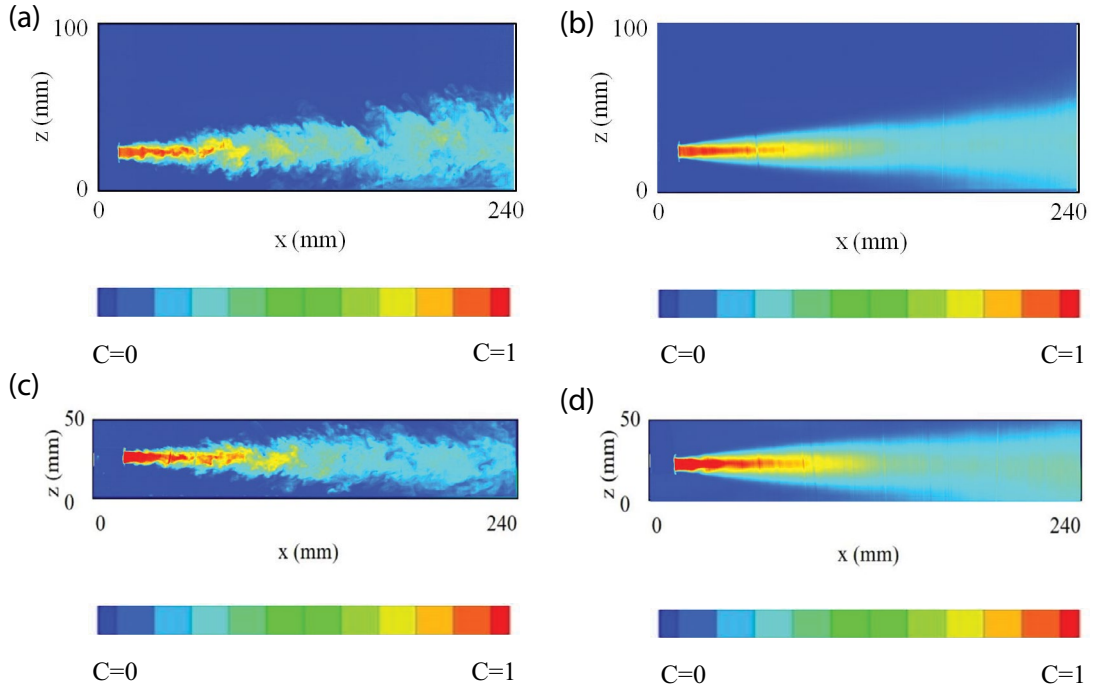

Fig. 3. Experimental results on concentration contour. (a) Instantaneous contour of Case 1, (b) time-averaged contour of Case 1, (c) instantaneous contour of Case 7, and (d) time-averaged contour of Case 7.

comparing the experimental and numerical results, it can be found that the two results agreed reasonably well with each other. The relatively large eddies with sizes bigger than the sub-grids were observable in the instantaneous CFD predictions using LES approach.

To quantitatively evaluate the CFD predictions, the non-dimensional jet trajectory was compared for all cases as shown in Fig. 5, where z/D = 0 represents the position of the bottom boundary. The jet trajectory refers to the concentration trajectory in the present study, which is the location of the maximum concentration at various cross sections [26]. It can be seen that the jet trajectory moved upward (i.e., Cases 1–5) and downward (i.e., Cases 6–8) for the positively and negatively buoyant jets, respectively. It was reported in previous studies that the jet trajectory deviated from the integral model prediction for unbounded flows due to the Coanda effect when the bed proximity parameter h/L_M was <0.1–0.15, where L_M is the jet characteristic length scale defined by $L_M = (\pi/4)^{0.25}$DFr [34,18]. Johnston and Volker [17] also noted that, compared to the buoyant jet in unbounded conditions, a delay in rising was observed even for non-Coanda flows when the boundary was sufficiently close to the jet. In the present study, the bed proximity parameter was about 0.1–0.2 as presented in Table 1. Although the complete Coanda attachment (i.e., the effluent adhered to the bottom after being discharged immediately) was not observed for all the experimental conditions, deviations with unbounded jets were expected with such small bed proximity parameters. From Fig. 5, it can be seen that the predicted jet trajectories agreed well with the experimental results within the measured distance of 20–30 D. This agreement suggested that the LES simulations are able to take into account the

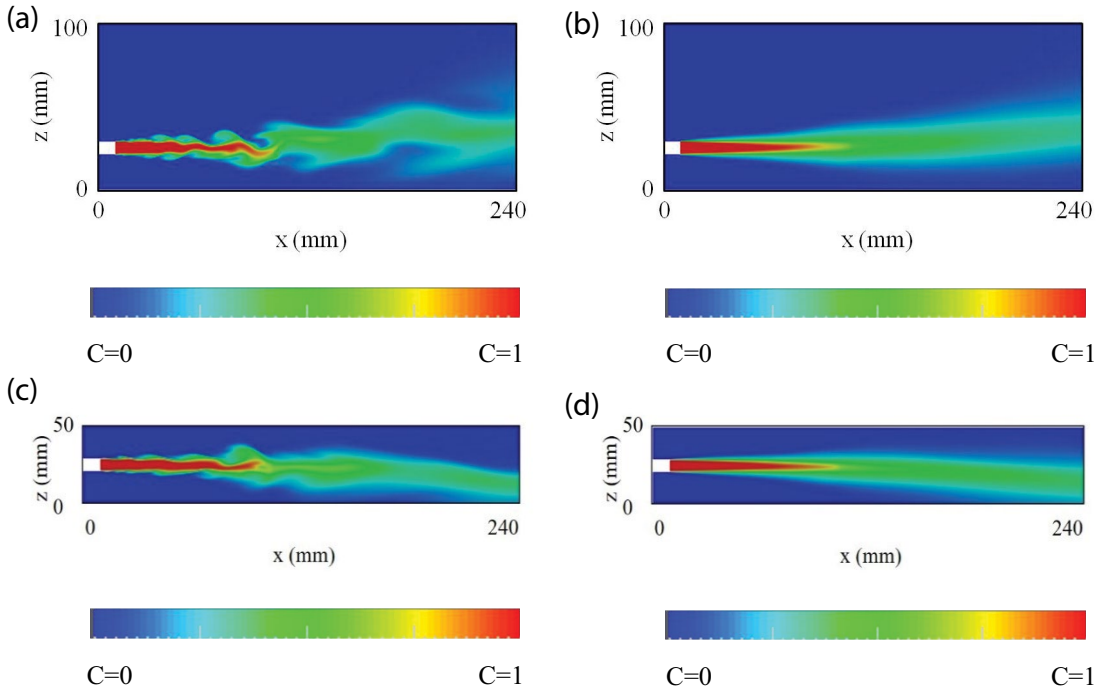

Fig. 4. Numerical predictions on concentration contour. (a) Instantaneous contour of Case 1, (b) time-averaged contour of Case 1, (c) instantaneous contour of Case 7, and (d) time-averaged contour of Case 7.

jet deviations induced by the shallow water conditions and potential Coanda effect, which overcomes the shortcoming of the integral models for unbounded jets. In addition, it was found that jets with the same Fr tend to behave similarly, while the trajectory becomes steeper for the cases with smaller Fr as expected (e.g., Case 2 vs. 5). This is reasonable as the Fr represents the ratio of flow inertia to the buoyancy effect. A smaller Froude number indicates potentially stronger buoyancy which leads to the faster rising/falling of the horizontal jet.

4.2. Mixing characteristics

To understand the environmental impact of the discharged effluents, the dilution of the jet is a critical parameter to be evaluated. Effluents with higher salinity (i.e., brine of desalination plants) or higher/lower temperature (i.e., cooling water of power plants and de-cooling water of LNG plants) than the ambient water have potentially adverse effects to the ocean environment and ecology [35]. Normally, a mixing zone is defined within which the salinity/temperature needs to be diluted to a certain value required by the local regulations.

Fig. 6 shows the non-dimensional concentration variation along the jet trajectory for all cases, where C_c is the local centerline concentration and C_0 the source concentration. It can be seen that C_c was generally maintained as the source concentration for a certain distance after the discharge (i.e., the potential core zone) and then decreased along the distance due to the entrainment of the ambient water. It should be noted that the experimental measurements very close to the exit were affected by the laser light reflection by the nozzle, which led to C_c/C_0 larger than one at some positions occasionally. In general, the numerical predictions and experimental measurements followed the same trend with a similar decreasing rate after the potential core zone.

It was reported by Johnston and Volker [17] that the potential core of a non-buoyant jet appeared to be shortened in shallow waters than that in unconfined conditions. The same observation was made by Shao and Law [21] for an offset dense jet. The present study confirms that for the jet with buoyancy, no matter positive or negative, the potential core tends to be shortened in the shallow water conditions as well. However, this phenomenon was not able to be captured by the current LES simulations satisfactorily; the predicted potential core zone was much longer (i.e., 7–8 D) compared to that of the measurements (i.e., 3–4 D). It is unclear whether this problem can be resolved by further refining the grid sizes at the area of potential core. However, a finer mesh requires an excessive amount of computing time, which shall be taken into consideration especially for the engineering applications.

For quantitative comparison, the minimum dilution at different locations, which is the source concentration divided by the local centerline concentration, that is, $S = C_0/C_c$, are presented in Table 3, where the results predicted by Visjet are also included for comparison. In particular, the dilution at x/D = 10 and 20 are calculated and compared. It can be seen that the predicted dilutions were slightly lower than the measurements, and the average underestimation was about 30% and 20% for the two locations, respectively. This result was consistent with Zhang et al. [26] where LES was applied for the prediction of inclined dense jets. The reason for the underestimation can be attributed to the fact that

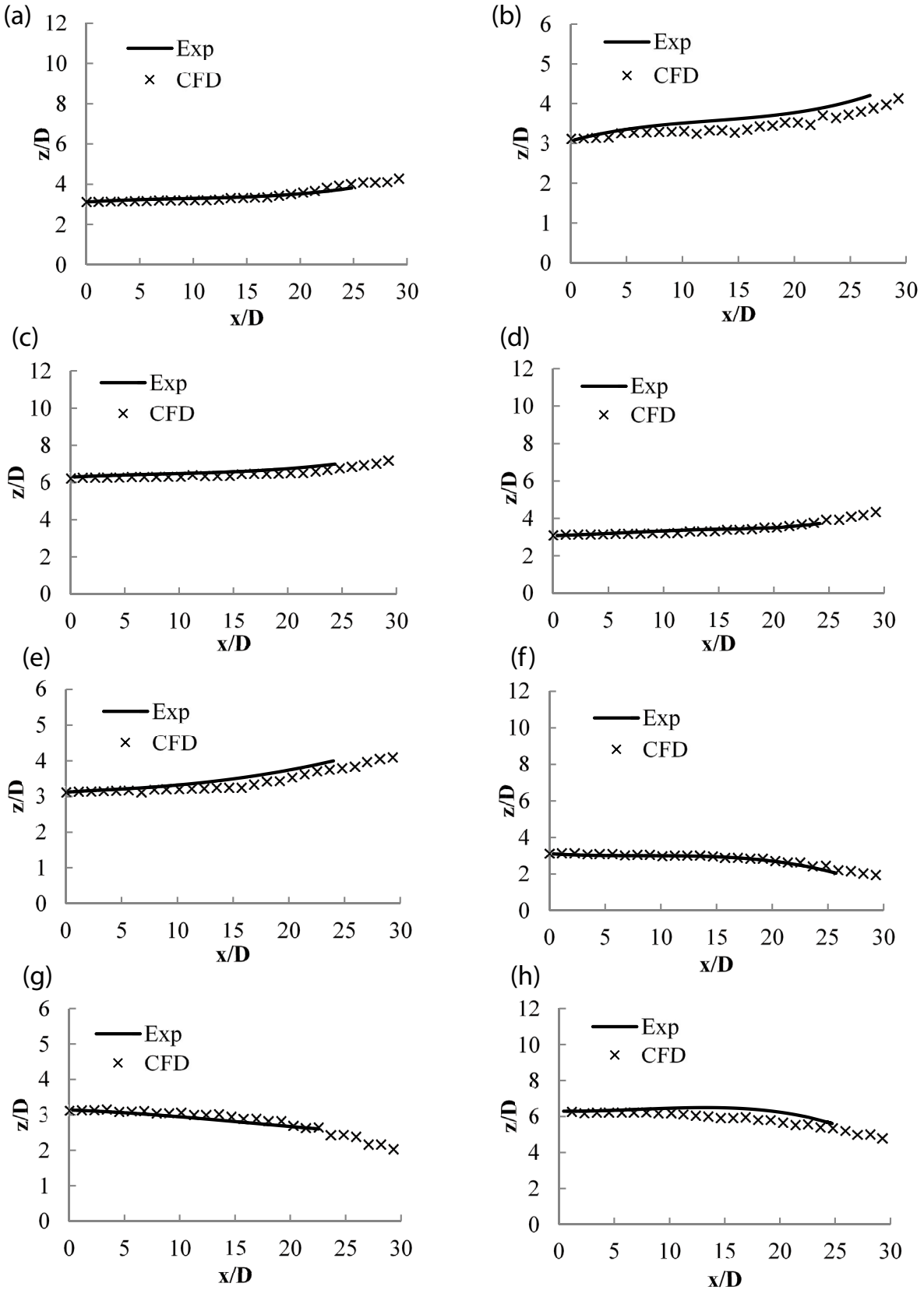

Fig. 5. Comparison on jet trajectory. (a) Case 1, (b) case 2, (c) case 3, (d) case 4, (e) case 5, (f) case 6, (g) case 7, and (h) case 8.

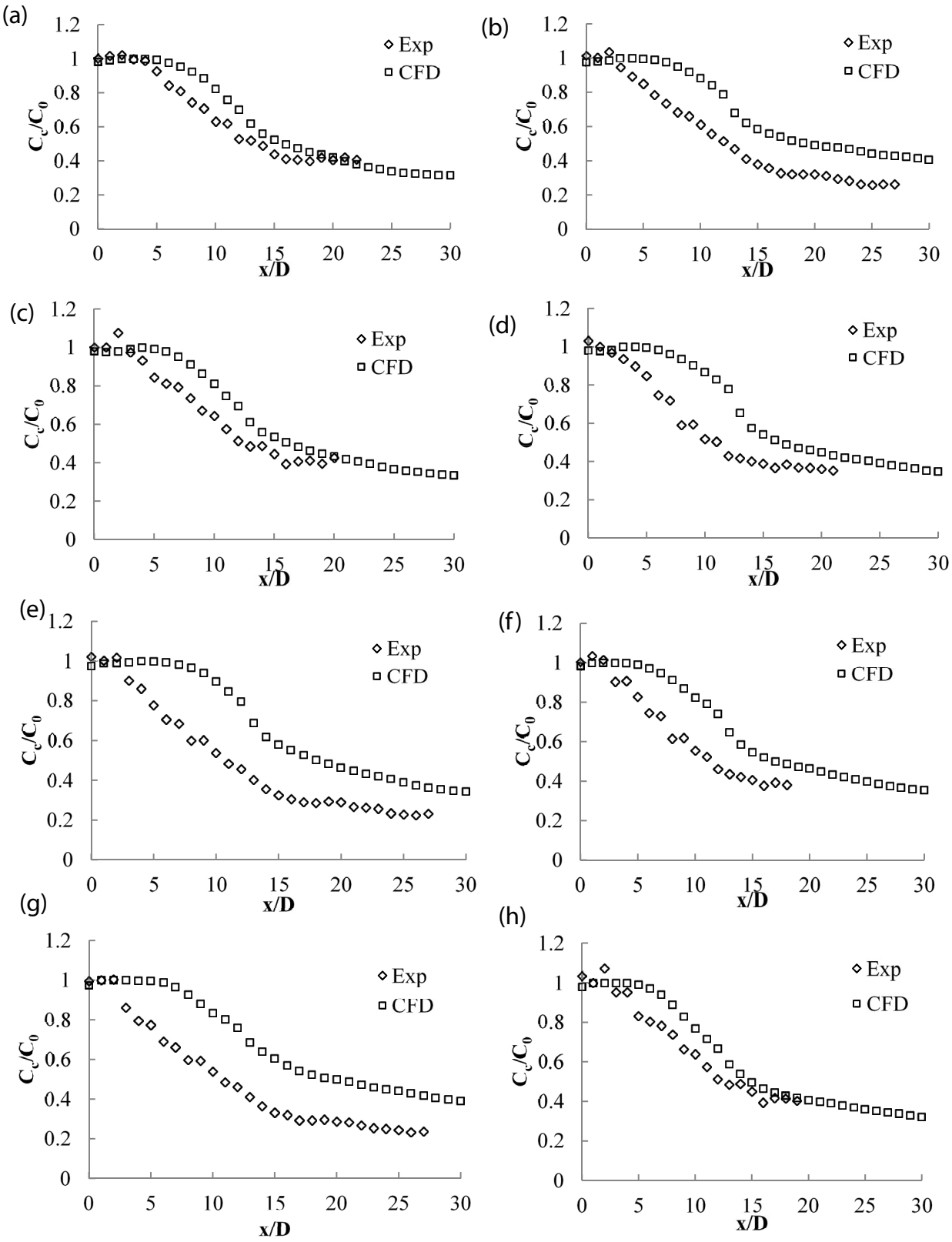

Fig. 6. Comparison on concentration variation along the trajectory. (a) Case 1, (b) case 2, (c) case 3, (d) case 4, (e) case 5, (f) case 6, (g) case 7, and (h) case 8.

Table 3
Comparison of minimum dilution at different locations

Case	x/D = 10 Exp	CFD	Visjet	x/D = 20 Exp	CFD	Visjet
1	1.58	1.22	2.49	2.47	2.38	4.39
2	1.63	1.14	2.50	3.12	2.03	4.39
3	1.55	1.24	2.50	2.35	2.33	4.39
4	1.93	1.15	2.48	2.77	2.24	4.40
5	1.86	1.12	2.48	3.46	2.15	4.42
6	1.80	1.21	2.49	2.53	2.15	4.42
7	1.85	1.20	2.49	3.47	2.01	4.43
8	1.56	1.30	2.49	2.33	2.47	4.42

the convective turbulence under the influence of buoyancy is difficult to be fully captured by the Smagorinsky SGS model [26]. Overall, the LES predictions are superior than that of Visjet, which are expected because Visjet is not developed for cases whereby the dilution is constrained by confined boundaries and thus results in a significant overestimation.

4.3. Cross sectional profiles and jet spread

Fig. 7 presents the comparison on the normalized concentration profile at the cross sections of x/D = 10 and 20 for Case 1, where C is the local concentration, r is the radial distance (positive and negative represent the lower and upper half, respectively), and b_c is the concentration spread width [12]. It can be found that both the predicted and observed cross-sectional concentration profiles distributed in the Gaussian manner and showed self-similarity. It should be noted that the density difference between the effluent and ambient water, which was generated by temperature difference in the present study, was much smaller compared to that of some previous studies on the inclined dense jets [27,10]. Thus, the concentration deviation from the Gaussian profile induced by the buoyancy effects was not obvious here. It was also noticed that the observed lower half of the profile at the cross section of x/D = 20 stopped at $r/b_c \approx 1.2$. This was because the plume was blocked by the bottom boundary within a relatively short distance.

The variation of concentration jet spread of Case 1 as a positively buoyant jet is plotted in Fig. 8. In general, it can be seen that the jet spread width increased with the distance. In the near-nozzle zone, the increase of the width was almost linear, and the upper and lower widths were almost identical. Beyond that, the upper width became larger than the lower width gradually, which was induced by the positive buoyancy (for a negatively buoyant jet, in an opposite way, the lower width became larger instead due to the negative buoyancy). In addition, the predicted upper and lower concentration spread widths can be observed to be smaller than that of the measurements, which implies that the predictions on the jet spread and ambient water entrainment were slower than the observations. This is consistent with the findings in Fig. 6 where the predicted centerline concentration decays more slowly. The reason is that the LES predictions may not be able to fully capture the buoyancy-induced instability due to the inadequacy of the SGS models.

4.4. Turbulence characteristics

The concentration turbulence intensity, as well as the velocity turbulence intensity in the longitudinal direction along the trajectory, are obtained by analyzing the instantaneous concentration and velocity fluctuation for all simulation cases as shown in Figs. 9 and 10, respectively, where C_{rms} and U_{rms} are the root mean square of concentration and horizontal velocity, and U_c the local horizontal velocity at the centerline. We note that the small duration for analysis was not sufficient to yield the ergodic properties of the fluctuations since the range of frequency was obviously inadequate [29]. Nevertheless, some qualitative observations can be made here. It can be seen that for both the concentration and velocity, the difference between the positively and negatively buoyant jets was not obvious. The concentration turbulence intensity of all cases showed self-similarity. It maintained at the same value of almost zero for a certain distance, that is, x/D = 5, and increased linearly until reaching the peak at about x/D = 12, and then decreased gradually in a wavy manner. The velocity turbulence intensity followed a similar pattern. However, different from the concentration, the velocity turbulence intensity started from the initial value of 0.1

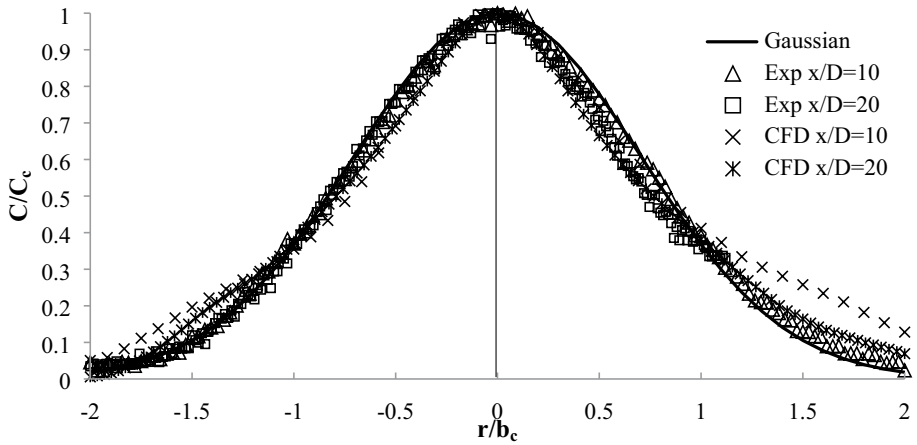

Fig. 7. Non-dimensional cross-sectional distributions of normalized concentration of Case 1.

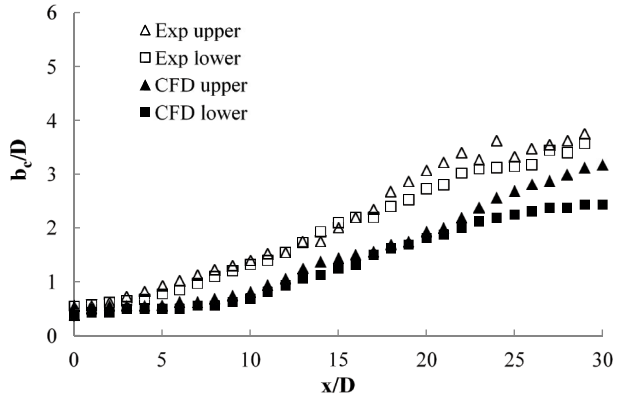

Fig. 8. Variation of upper and lower concentration spread widths along the trajectory of Case 1.

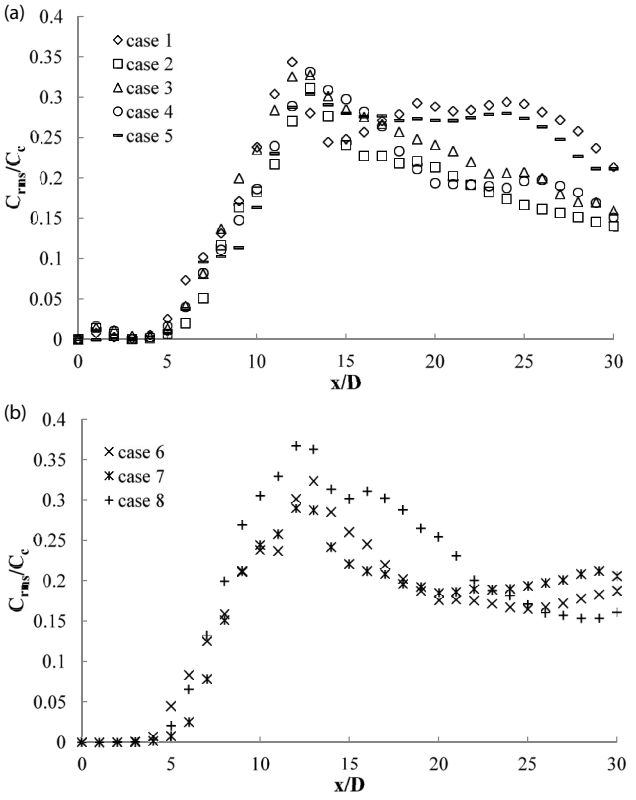

Fig. 9. Concentration turbulence intensity along the trajectory. (a) Positively buoyant jets and (b) negatively buoyant jets.

which was set at the outlet boundary. It slightly decreased for a short distance and then increased until reaching the peak value of 0.25–0.3, which was lower than that of the concentration turbulence intensity.

In addition, the cross-sectional concentration and velocity turbulence intensities at various cross sections of Case 1 is plotted in Fig. 11. All the cross-sectional concentration turbulence intensity followed a similar trend. The twin peaks can be observed with one on each side of the centerline at the position of $r/b_c \approx \pm 0.5$. Similar results can be observed for the cross-sectional velocity turbulence intensity but with the peak

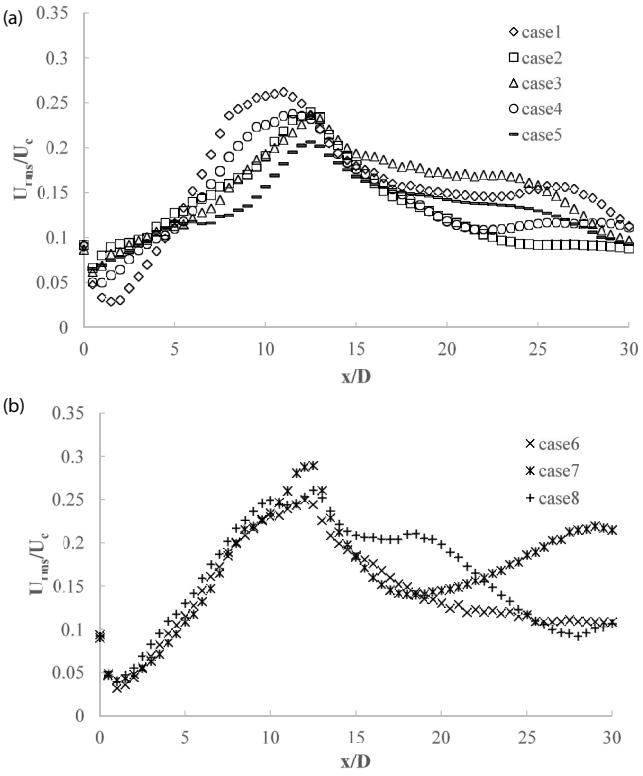

Fig. 10. Velocity turbulence intensity along the trajectory. (a) Positively buoyant jets and (b) negatively buoyant jets.

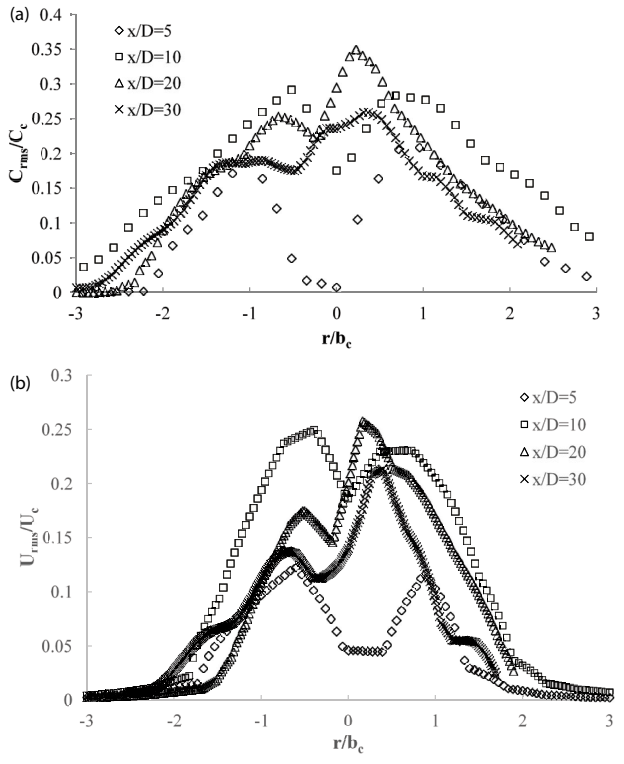

Fig. 11. Cross-sectional turbulence intensity at different locations of Case 1. (a) Concentration and (b) velocity.

values as well as the span width lower than that of the concentration. In general, the velocity field had relatively weaker turbulence fluctuations both longitudinally and transversely, which implied that the buoyancy-induced instability has a stronger effect to the concentration fluctuation.

5. Conclusions

In this case study, submerged horizontal jets with either positive or negative buoyancy in shallow waters were investigated both numerically by using the LES approach and experimentally by PLIF. The experimental results showed that the potential core zone of the jet with buoyancy is relatively shorter in shallow waters compared to that in unbounded conditions. In general, the LES simulations are able to reproduce the geometric characteristics of the jet with buoyancy satisfactorily with visualization of eddies. Specifically, the jet trajectory in shallow water conditions with potential Coanda effect, which deviates from that in unconfined conditions, can be predicted in a satisfactory manner. However, the predicted potential core zone tends to be longer and the spreading rate is slower compared to the measurement. The predicted dilution is underestimated by 20%–30% depends on the locations, which can be attributed to the SGS model limitations. This study shows that, for the conditions of shallow water where the conventional integral models (e.g., Visjet, Cormix, etc.) are not suitable to be employed, the numerical model with LES approach is a feasible and more reliable way for the engineering company to examine the jet characteristics as well as the mixing performance when assessing the environmental impact and outfall design of the industrial facilities (e.g., desalination, power, and LNG plants). It should also be noted that the merging effect of the multiple jets, as well as the interaction with boundaries, were not fully investigated due to the experimental constraints in this study. Future studies with longer observation distances and spanwise measurements to address the merging effect of multiple jets with buoyancy in shallow waters need to be conducted.

Symbols

b_c	—	Concentration spread width
C	—	Concentration
C_c	—	Centerline concentration
C_{rms}	—	Root mean square of concentration
C_S	—	Smagorinsky constant
C_0	—	Source concentration
d	—	Distance from port center to water surface
d_{wall}	—	Distance to the wall
D	—	Port diameter
Fr	—	Densimetric Froude number
g	—	Gravitational acceleration
h	—	Distance from port center to bottom
L_M	—	Jet characteristic length scale
L_S	—	Mixing length
p	—	Pressure
Q_j	—	SGS scalar flux
r	—	Radial distance
Re	—	Reynolds number
S	—	Dilution
$\tilde{S}_{ij}$	—	Strain rate tensor
Sc_t	—	Turbulent Schmidt number
t	—	Time
T_a	—	Ambient temperature
T_e	—	Effluent temperature
u_0	—	Exit velocity
u_i	—	Velocity in i direction
u_j	—	Velocity in j direction
U_c	—	Local centerline velocity at x direction
U_{rms}	—	Root mean square of velocity at x direction
x	—	Horizontal direction
z	—	Vertical direction
μ	—	Dynamic viscosity
μ_t	—	SGS viscosity
ν	—	Kinematic viscosity
ρ	—	Fluid density
ρ_a	—	Ambient density
$\Delta\rho$	—	Density difference
$\tau_{i,j}$	—	SGS stress
τ_{kk}	—	Isotropic part of the SGS stress
κ	—	Von Karman constant
Γ	—	Scalar diffusivity
ϕ	—	Scalar concentration
Δ	—	Grid size

References

[1] P.J.W. Roberts, A. Ferrier, G. Daviero, G., Mixing in inclined dense jets, J. Hydraul. Eng., 123 (1997) 693–699.
[2] G.H. Jirka, Improved discharge configurations for brine effluents from desalination plants, J. Hydraul. Eng., 134 (2008) 116–120.
[3] I.G. Papakonstantis, G.C. Christodoulou, Spreading of round dense jets impinging on a horizontal bottom, J. Hydro-environ. Res., 4 (2010) 289–300.
[4] J.H.W. Lee, Mixing of multiple buoyant jets, J. Hydraul. Eng., 138 (2012) 1008–1021.
[5] G.H. Jirka, R.L. Doneker, Hydrodynamic classification of submerged single-port discharges, J. Hydraul. Eng., 117 (1991) 1095–1112.
[6] P. Palomar, J.L. Lara, I.J. Losada, Near field brine discharge modeling part 2: validation of commercial tools, Desalination, 290 (2012) 28–42.
[7] C.C.K. Lai, J.H.W. Lee, Mixing of inclined dense jets in stationary ambient, J. Hydro-environ. Res., 6 (2012) 9–28.
[8] T. Bleninger, G.H. Jirka, Modelling and environmentally sound management of brine discharges from desalination plants, Desalination, 221 (2008) 585–597.
[9] A.B. Pincince, E.J. List, Disposal of brine into an estuary, J. Water Pollut. Control Fed., 45 (1973) 2335–2344.
[10] G.A. Kikkert, M.J. Davidson, R.I. Nokes, Inclined negatively buoyant discharges, J. Hydraul. Eng., 133 (2007) 545–554.
[11] A. Cipollina, A. Brucato, F. Grisafi, S. Nicosia, Bench-scale investigation of inclined dense jets, J. Hydraul. Eng., 131 (2005) 1017–1022.
[12] M.T. Jiang, A.W.K. Law, S. Zhang, Mixing behavior of 45° inclined dense jets in currents, J. Hydro-environ. Res., 18 (2018) 37–48.
[13] E.E. Adams, A.D. Koussis, Transient analysis for shallow cooling ponds, J. Energy Div., 106 (1980) 141–153.
[14] D.Y. Chen, G.H. Jirka, LIF study of plane jet bounded in shallow water layer, J. Hydraul. Eng., 125 (1999) 817–826.
[15] J.P. Raiford, A.A. Khan, Investigation of circular jets in shallow water, J. Hydraul. Res., 47 (2009) 611–618.
[16] A.M. Shinneeb, R. Balachandar, J.D. Bugg, Confinement effects in shallow-water jets, J. Hydraul. Eng., 137 (2011) 300–314.
[17] A.J. Johnston, R.E. Volker, Round buoyant jet entering shallow water, J. Hydraul. Res., 31 (1993) 121–138.

[18] R.J. Sobey, A.J. Johnston, R.D. Keane, Horizontal round buoyant jet in shallow water, J. Hydraul. Eng., 114 (1988) 910–929.
[19] B.X. Jiang, A.W.K. Law, J.H.W. Lee, Mixing of 30° and 45° inclined dense jets in shallow coastal waters, J. Hydraul. Eng., 140 (2014) 241–253.
[20] D.D. Shao, A.W.K. Law, Turbulent mass and momentum transport of a circular offset dense jet, J. Turbul., 10 (2009) 1–24.
[21] D.D. Shao, A.W.K. Law, Boundary impingement and attachment of horizontal offset dense jets, J. Hydro-environ. Res., 5 (2011) 15–24.
[22] S. Nemlioglu, N. Sezgin, Water depth effects on initial dilution of horizontally discharged cold water from an elevated outfall, Int. J. Global Warming, 6 (2014) 284–294.
[23] N. Sezgin, Investigation of horizontal cold water discharge initial dilutions at various temperature differences using duckbill valve, Desalin. Water Treat., 57 (2016) 2437–2445.
[24] U.E. Temilli, N. Sezgin, F. Djamaa, S. Nemlioglu, An investigation on initial dilution of thermal wastewater discharges into shallow receiving waters with 60° inclination, Desalin. Water Treat., 93 (2017) 355–360.
[25] Y.H. Zeng, W.X. Huai, Numerical study on the stability and mixing of vertical round buoyant jet in shallow water, Appl. Math. Mech., 26 (2005) 92–100.
[26] S. Zhang, B. Jiang, A.W.K. Law, B. Zhao, Large eddy simulations of 45 inclined dense jets, Environ. Fluid Mech., 16 (2016) 101–121.
[27] C. Oliver, M. Davidson, R. Nokes, k-ε Predictions of the initial mixing of desalination discharges, Environ. Fluid Mech., 8 (2008) 617–625.
[28] M.N. Chowdhury, A.A. Khan, F.Y. Testik, Numerical investigation of circular turbulent jets in shallow water, J. Hydraul. Eng., 143 (2017) 04017027.
[29] A.W.K. Law, H.W. Wang, Measurement of mixing processes with combined digital particle image velocimetry and planar laser induced fluorescence, Experim. Therm. Fluid Sci., 22 (2000) 213–229.
[30] P. Baj, P.J.K. Bruce, O.R.H. Buxton, On a PLIF quantification methodology in a nonlinear dye response regime, Experim. Fluids, 57 (2016) 106.
[31] J. Smagorinsky, General circulation experiments with the primitive equations, Mon. Weather Rev., 91 (1963) 99–164.
[32] A.W.K. Law, Velocity and concentration distributions of round and plane turbulent jets, J. Eng. Math., 56 (2006) 69–78.
[33] D.K. Lilly, The Representation of Small Scale Turbulence in Numerical Simulation Experiments, Proceedings of IBM Scientific Computing Symposium on Environmental Sciences, Yorktown Heights, New York, 1967, pp. 195–210.
[34] J.J. Sharp, B.D. Vyas, The buoyant wall jet, Proc. Inst. Civ. Eng. 63 (Pt 2) (1977) 593–611.
[35] M. Milione, C. Zeng, The effects of temperature and salinity on population growth and egg hatching success of the tropical calanoid copepod, *Acartia sinjiensis*, Aquaculture, 275 (2008) 116–123.